

# Comparing Direct Observation of Strain, Rotation, and Displacement with Array Estimates at Piñon Flat Observatory, California

by Stefanie Donner, Chin-Jen Lin, Céline Hadziioannou, André Gebauer, Frank Vernon, Duncan Carr Agnew, Heiner Igel, Ulrich Schreiber, and Joachim Wassermann

## ABSTRACT

The unique instrument setting at the Piñon Flat Observatory in California is used to simultaneously measure 10 out of the 12 components, completely describing the seismic-wave field. We compare the direct measurements of rotation and strain for the 13 September 2015  $M_w$  6.7 Gulf of California earthquake with array-derived observations using this configuration for the first time. In general, we find a very good fit between the observations of the two measurements with cross-correlation coefficients up to 0.99. These promising results indicate that the direct and array-derived measurements of rotation and strain are consistent. For the array-based measurement, we derived a relation to estimate the frequency range within which the array-derived observations provide reliable results. This relation depends on the phase velocity of the study area and the calibration error, as well as on the size of the array.

## INTRODUCTION

According to the theory of infinitesimal deformation, three components of translation, three components of rotation, and six components of strain are needed to completely describe the local motion of a deformable body (e.g., Aki and Richards, 2002). Nevertheless, seismology is primarily based on the observation, processing, and inversion of the three components of translation. It has been shown in previous theoretical and numerical studies that using additional observables can be of great benefit for several seismological applications (e.g., Bernauer *et al.*, 2012, 2014; Donner *et al.*, 2016; Reinwald *et al.*, 2016). However, all 12 components of the elastic wavefield have not been observed simultaneously at a single location yet.

In a unique instrument setting at Piñon Flat Observatory (PFO), California, a dense seismic array is collocated with a vertical-component ring laser gyroscope (RLG), as well as a three-component long-base laser strainmeter (LSM). This allows us to measure seven out of nine independent components of the elastic wavefield. In this study, we analyze a teleseismic earthquake recorded at PFO, where four components of strain

and the vertical component of rotation are measured by two independent methods, that is, direct observation and array-derived measurements. Thus, we can evaluate the consistency of translation, rotational, and strain observations.

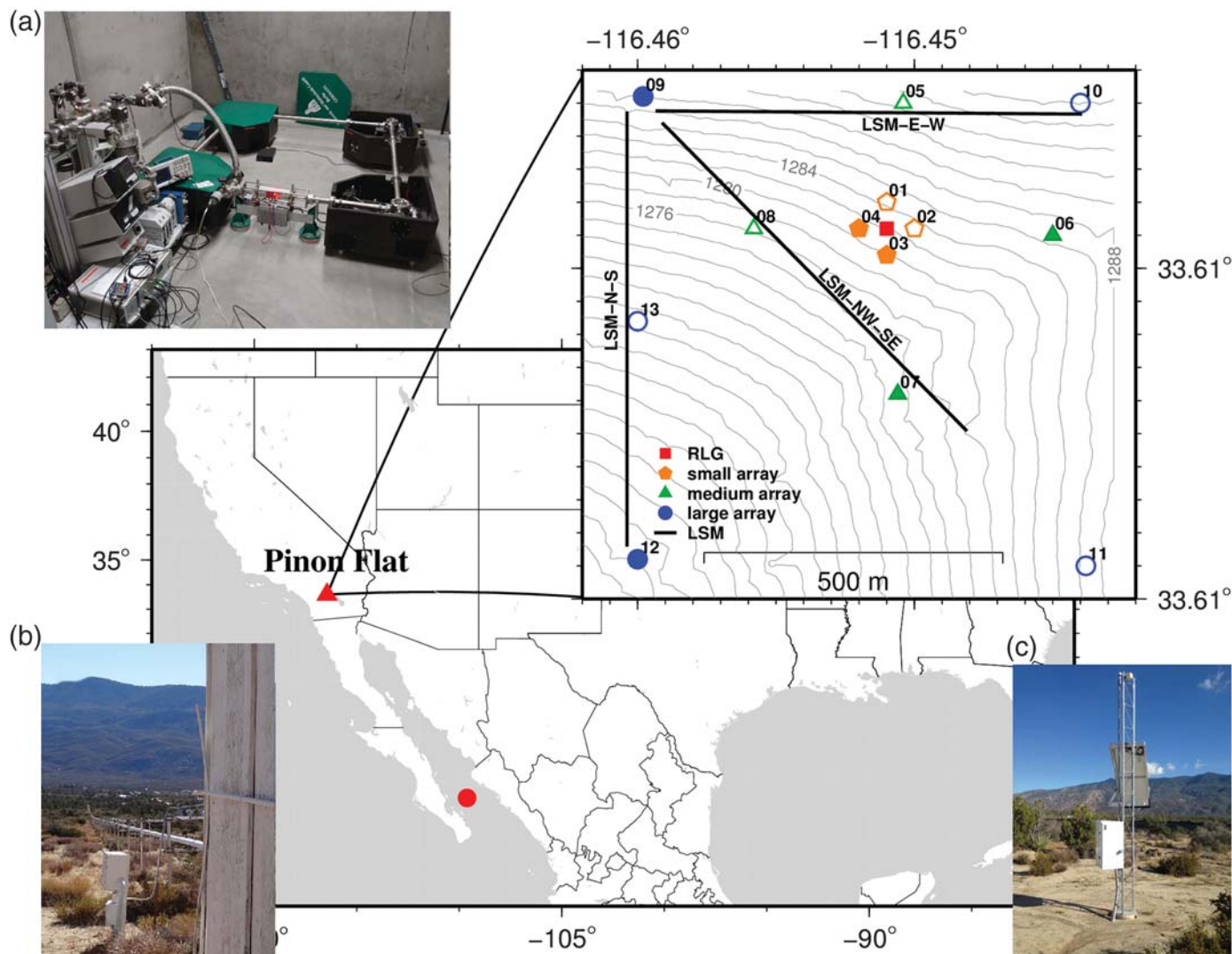
In previous studies, direct observations have been compared with array-derived rotations (Suryanto *et al.*, 2006; Wassermann *et al.*, 2009; Lin *et al.*, 2012) and strain (Langston and Liang, 2008). However, such comparisons have never been performed simultaneously.

Compared with data from translational seismometers, observations from rotational instruments are only available over the last decade. Direct observation of ground rotation for teleseismic events is difficult, mainly due to sensor sensitivity. So far, only the RLG technique has low enough noise to observe ground rotation in a broad frequency band (Schreiber *et al.*, 2009). There are substantial benefits from collocated recordings of seismometer and vertical-component RLG, for example, estimation of the shear-wave phase velocity from a single-point measurement (Igel *et al.*, 2005), determining phase velocity and back azimuth from rotational ambient noise (Hadziioannou *et al.*, 2012), identifying Love-wave energy in the secondary microseism (Tanimoto *et al.*, 2015), determining near-receiver structure (Bernauer *et al.*, 2012), and improving the parameter resolution during source inversion (Bernauer *et al.*, 2014; Donner *et al.*, 2016; Reinwald *et al.*, 2016).

In this study, we first discuss the limitations of array-derived rotation and strain. We focus, in particular, on how the calibration error limits the retrieval of the long wavelengths. Based on the array aperture and the local wave velocity, we define a reliable frequency range for the array-derivation method. In the second part, we show and discuss the comparison of array-derived with direct observation of rotation and strain for the 13 September 2015  $M_w$  6.7 Gulf of California earthquake.

## INSTRUMENTATION AT PFO

The instrumental setting at PFO can be seen in Figure 1. It includes a seismic array with a collocated vertical-component



▲ **Figure 1.** Instrumental setting at Piñon Flat Observatory (red triangle on overview map). Red dot marks the epicenter of the analyzed earthquake. The 13 seismic stations are color coded according to array aperture. Station 01 is selected as the center station. Stations marked by filled and open symbols are equipped with Nanometrics Trillium 120PH and STS-5A seismometers, respectively. The vertical component of the ring laser gyroscope (RLG) is marked by a red square. The three-component long-base laser strainmeters (LSMs) are indicated by lines labeled according to their orientation north–south (N–S), east–west (E–W), and northwest–southeast (NW–SE). Gray lines give digital elevation model topography in steps of 2 m. (a) Photo of the RLG, (b) photo of one of the LSM, and (c) photo of one of the seismic stations.

RLG and a three-component LSM. The array is composed of 13 broadband stations (network name PY) and was deployed in February 2014. Seven stations are equipped with STS-5A seismometers and six with Nanometrics Trillium 120PH seismometers; both have a low-frequency corner of 120 s. All seismometers are connected to Quanterra Q330S+ recorders (sample rate 20 Hz, number of bits 32) and are installed in holes with depths of 2–3 m. The array can be divided into subarrays with three different apertures (90, 495, and 776 m) and, in total, covers the entire area of the RLG and the LSM.

The vertical-component RLG was installed in the center of the seismic array in 2005 (Velikosevtsev, 2005; Schreiber *et al.*, 2006, 2009). It was designed to meet the requirements of reliably measuring rotational ground motion while keeping the construction costs low. The side length of the square ring

laser is 1.6 m (enclosed area 2.56 m<sup>2</sup>). It is sampled at 20 Hz with 24-bit resolution. The flat frequency response, high resolution, and insensitivity to translational motion make the ring-laser technique attractive for studies of ground rotation.

The three long-base LSMs measure extensional strains over 732 m paths oriented north–south, east–west, and northwest–southeast (NW–SE). These instruments use optical interferometers with a nominal resolution of  $1.08^{-10}$  in strain; the calibrations, being based on the wavelength of light, are accurate to 0.1% (Berger and Lovberg, 1970; Agnew and Wyatt, 2003). The data are recorded at 1 Hz, after analog prefiltering with a four-pole RC filter with time constant 0.5 s, and with each instrument using a separate datalogger/control system. The NW–SE instrument was not operating at the time of the earthquake analyzed here, so instead a shorter (200 m) optical-fiber

system of the type described by DeWolf *et al.* (2015) was used; this instrument was installed parallel to the NW–SE longer instrument. It also applies interferometric measurements, but uses the fringe-follower system described by Zumberge *et al.* (2004), with initial sampling at 50 kHz followed by digital filtering to 50 Hz sampling with 54-bits resolution.

## ARRAY-DERIVED GRADIENT, STRAIN, AND ROTATION

Assuming infinitesimal deformation, the displacement  $\mathbf{u}$  of a point  $\mathbf{x}$  in relation to its neighboring point  $\mathbf{x} + \delta\mathbf{x}$  can be expressed by

$$\begin{aligned} \mathbf{u}(\mathbf{x} + \delta\mathbf{x}) &= \mathbf{u}(\mathbf{x}) + \mathbf{G}\delta\mathbf{x} \\ &= \mathbf{u}(\mathbf{x}) + \epsilon\delta\mathbf{x} + \Omega\delta\mathbf{x} = \mathbf{u}(\mathbf{x}) + \epsilon\delta\mathbf{x} + \omega \times \delta\mathbf{x}, \end{aligned} \quad (1)$$

with  $\mathbf{G}$ ,  $\epsilon$ , and  $\Omega$  being the gradient, strain, and rotation second-order tensors, respectively.  $\omega$  is a (pseudo-)vector giving the angle of (rigid) rotation (Cochard *et al.*, 2006).

Spudich *et al.* (1995) described an array method to determine uniform strain and rigid body rotation of a wavefield. Because of the zero traction condition at the free surface, the two vertical components of shear strains ( $e_{zr}$ ,  $e_{zt}$ ) are forced to be zero. In addition, the vertical strain component ( $e_{zz}$ ) can be obtained by the orthogonal normal components of strain ( $e_{rr}$ ,  $e_{tt}$ ) at the surface (Romney, 1964; Cochard *et al.*, 2006). Thus, four components of strain and three components of rotation can be determined using the array-derivation method. Along with the three components of translation, 10 out of 12 components describing the complete wavefield of ground motion can be derived.

Given the array measurements and the relative distances of the stations, an array-derived gradient matrix  $\mathbf{G}$  with displacements  $u_{ij}$  can be obtained in the radial-transverse system by

$$\mathbf{G} = \begin{bmatrix} u_{r,r} & u_{r,t} & u_{r,z} \\ u_{t,r} & u_{t,t} & u_{t,z} \\ -u_{r,z} & -u_{t,z} & -\eta(u_{r,r} + u_{t,t}) \end{bmatrix}, \quad (2)$$

in which  $\eta = 1 - (2V_S^2/V_P^2)$ , and  $V_P$  and  $V_S$  are the velocities of  $P$  and  $S$  waves, respectively. Based on the assumptions of zero traction and plane-wave propagation, the rotation vector and strain tensor are thus obtained as

$$\begin{bmatrix} \omega_r \\ \omega_t \\ \omega_z \end{bmatrix} = \begin{bmatrix} u_{z,t} \\ -u_{z,r} \\ -\frac{1}{2}(u_{r,t} - u_{t,r}) \end{bmatrix} \quad (3)$$

and

$$\begin{bmatrix} e_{rr} \\ e_{tt} \\ e_{zz} \\ e_{zr} \\ e_{zt} \\ e_{rt} \end{bmatrix} = \begin{bmatrix} u_{r,r} \\ u_{t,t} \\ -\eta(u_{r,r} - u_{t,t}) \\ 0 \\ 0 \\ \frac{1}{2}(u_{r,t} + u_{t,r}) \end{bmatrix} \quad (4)$$

(e.g., Spudich *et al.*, 1995; Shearer, 2009).

At this point, we want to make clear that although all the developments are in terms of displacement, strain, and rotation, what is shown in the following is rates, because that is what the RLG measures.

## Limitations of the Array-Derivation Method

When performing array calculations, the aperture and the phase velocity limits the frequency range of the derived rotation and strain signal. For the upper-frequency limit, to prevent spatial aliasing and keep uniform strain across the array, Spudich and Fletcher (2008) argue that the array aperture should be smaller than a quarter of the considered wavelength. For the lower-frequency limit, the calibration error in the seismograms due to inaccuracies in the specification of sensitivity of the recording system limits the retrieval of long-period wavelengths (Poppeliers and Evans, 2015; Ringer *et al.*, 2016).

To find a lower-frequency limit, we generally follow the approach of Spudich and Fletcher (2008) and Poppeliers and Evans (2015). They have evaluated the amplitude differences in the wavefield gradient from peak to peak. However, we chose to evaluate the values at the zero crossing to broaden the range of frequencies available in the analysis. Together with a calibration error of 1.5% (empirically obtained using four collocated STS-2 seismometers, see Appendix A), we obtain an amplitude error of about 0.2%. Thus, the frequency limits for obtaining reliable array derived results can be given as

$$\frac{0.00238 \cdot c}{b} < f < \frac{0.25 \cdot c}{b} \quad (5)$$

with  $f$  and  $c$  being the frequency and the apparent velocity of the seismic wave along the Earth's surface, respectively, and  $b$  is the array aperture.

We want to emphasize that the lower-frequency bound derived here is a very optimistic one. However, the results show that it is a fair estimate for this study. For a more conservative estimate, we refer to Poppeliers and Evans (2015) and Langston (2007a,b).

## DATA PROCESSING

Here, we estimate a reliable frequency range for the array-derivation method for the PFO array using the relations developed earlier. First, we substitute the size of the medium aperture array (495 m) and an averaged phase velocity of 3800 m/s (Prieto *et al.*, 2009; Barbour and Agnew, 2012) into equation (5), the frequency range is then determined as 0.018–1.92 Hz. The analog antialias filter of the LSM has its corner frequency at 0.32 Hz (Agnew and Wyatt, 2014), below the upper limit of this frequency range. To take this corner frequency into account, we limit the frequency range to 0.018–0.32 Hz.

Before performing the array derivation, all seismograms are corrected for the nominal instrument response, band-pass filtered within the determined frequency range, and corrected for the relative orientations with respect to the center station (see Appendix B). The velocity data of the center station are time differentiated to obtain acceleration, which is propor-

tional to strain and rotation rate (e.g., Igel *et al.*, 2005). The array derivation has been done using the Python-based ObsPy toolbox `signal.array_rotation_strain` (Beyreuther *et al.*, 2010; Megies *et al.*, 2011; Krischer *et al.*, 2015).

For the RLG, the instantaneous frequency of the Sagnac interferogram was estimated using the Hilbert transform, down-sampled to the same sampling rate of the seismograms, and calibrated for the instrumental scale factor to obtain rotation rate (Velikoseltsev, 2005). The LSM data are corrected for the gain factor. Because the NW component of the LSM was not operational during the earthquake, this component is replaced by a collocated fiber strainmeter measurement (DeWolf *et al.*, 2012). The original strain data are time differentiated to strain rate. To have a uniform frequency response between the direct observations and the array derivations, RLG and LSM data are filtered with the same passband as the translation data.

The strain tensor transformation to obtain components in the vertical, radial, transverse (ZRT) coordinate system is described in Gombert and Agnew (1996) and Agnew and Wyatt (2014):

$$\begin{bmatrix} e_{rr} \\ e_{tt} \\ e_{rt} \end{bmatrix} = \begin{bmatrix} \cos^2 \phi & \sin^2 \phi & 2 \sin \phi \cos \phi \\ \sin^2 \phi & \cos^2 \phi & -2 \sin \phi \cos \phi \\ -\sin \phi \cos \phi & \sin \phi \cos \phi & \sin^2 \phi - \cos^2 \phi \end{bmatrix} \cdot \begin{bmatrix} e_{NS} \\ e_{EW} \\ e_{NW} \end{bmatrix}, \quad (6)$$

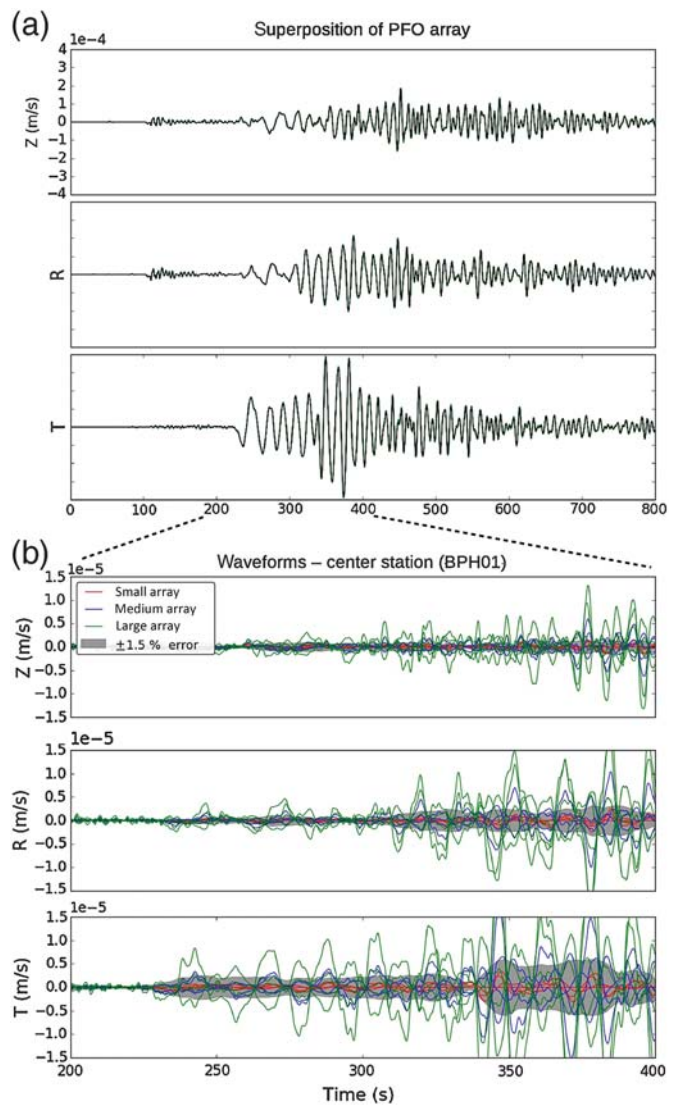
in which  $\phi$  is the azimuth from the receiver to source measured clockwise from north, and  $e_{NS}$ ,  $e_{EW}$ , and  $e_{NW}$  are measurements of the LSM along the instrument direction. Although it measures three horizontal strains on the surface, assuming a homogeneous medium and plane-stress condition, the vertical strain  $e_{zz}$  is derived using

$$e_{zz} = \frac{-\nu}{1-\nu} (e_{rr} + e_{tt}), \quad (7)$$

in which  $\nu$  is the local Poisson's ratio. It also means that the two vertical shear strains ( $e_{rz}$  and  $e_{tz}$ ) are zero (Agnew and Wyatt, 2014). A recent study by DeWolf *et al.* (2015) showed a consistent vertical strain measurement between fiber-based vertical strainmeter and LSM at PFO, yielding a Poisson's ratio of 0.25.

## OBSERVATIONS FOR THE 2015 $M_w$ 6.7 GULF OF CALIFORNIA EARTHQUAKE

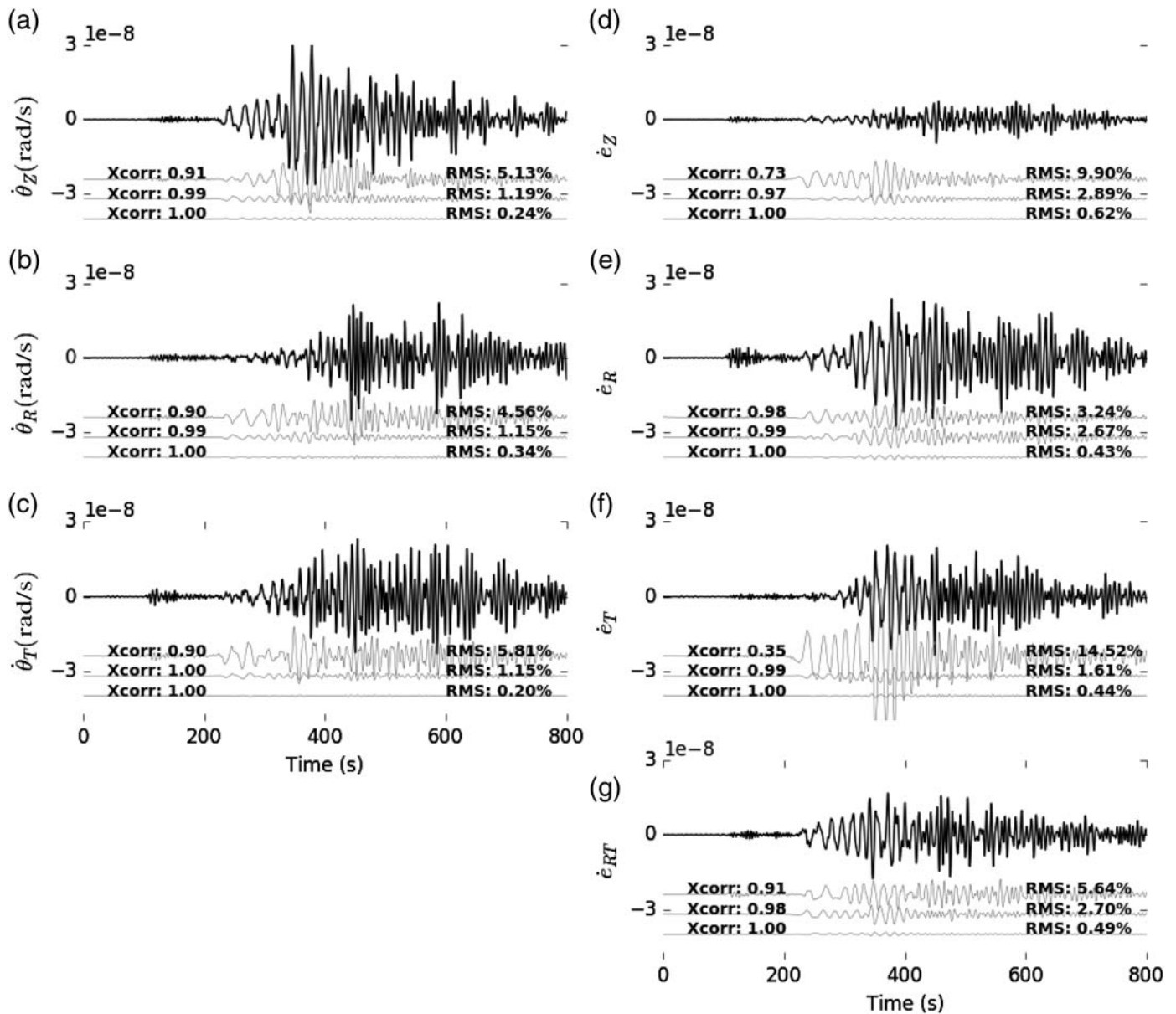
The 13 September 2015  $M_w$  6.7 Gulf of California earthquake (08:14 UTC, 24.91° N, 109.62° W, epicentral distance at 1169 km) was recorded simultaneously by all 13 seismic stations. The superposition of all instrument corrected seismograms in the radial-transverse system is shown in Figure 2. To see the influence of the array size, we do not filter these waveforms, for now. As expected, the seismograms are comparable in their amplitudes and general shape, indicating no major errors due to misalignment, timing error, instrument problems, or site response. To evaluate the discrepancy among the seismograms, the signal of the center station (01) is subtracted from all seismo-



▲ **Figure 2.** Superposition of all seismograms for the Gulf of California earthquake. (a) All seismograms superimposed. (b) Difference of the data from each station subtracted by the data of the central station (01) within the time window for Love waves. The differences are color coded according to the array apertures (see figure legend). A range of  $\pm 1.5\%$  of the amplitude envelope of the central station is shown in gray as a reference.

grams. In Appendix A, we show that the calibration error of the seismograms might be up to 1.5% of the amplitude envelope of the central station. As seen in Figure 2, the amplitude differences of the stations of the small subarray fall within this 1.5% range. Therefore, deriving rotation and strain from data of only the small subarray might not be reliable.

For the array derivation in the following, we applied the band-pass filter determined before. Figure 3 shows the superposition of array-derived rotation and strain for the three different subarray apertures and using all stations. It appears that the larger subarray obtains more consistent results, whereas the smaller subarray is prone to errors. The results for the medium subarray lie somewhere in between these two.



▲ **Figure 3.** (a–c) Array-derived rotation and (d–g) strain. Thick lines show results using the entire array. Thin lines show the differences to results using the (top) small, (center) medium, and (bottom) large array. They are quantified by the normalized root mean square (rms) deviation and the normalized cross-correlation coefficients (Xcorr).

### Comparison of Array-Derived with Direct Observations

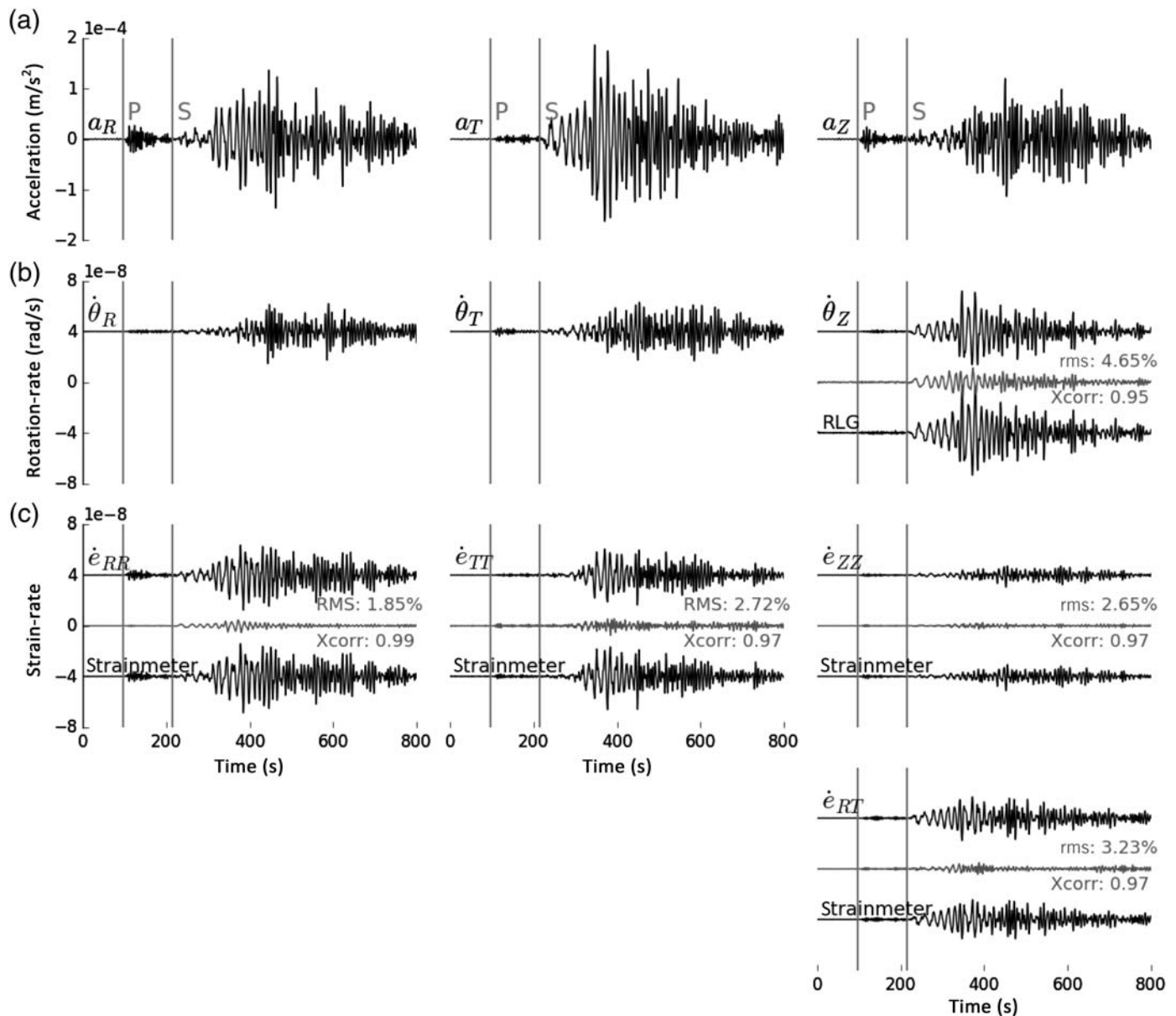
In Figure 4, we show the comparison of the array-derived, and direct observations, for the 2015  $M_w$  6.7 Gulf of California earthquake, whenever possible. The array-derived observations are based on the entire array using the data of all 13 stations. To quantify the differences between the signals for direct and array-derived observations, the normalized root mean square deviation and the normalized cross-correlation coefficients (Xcorr) are given.

In general, the comparison shows a very good and consistent fit between the two observation methods. Especially for the strain components, cross-correlation coefficients larger than 0.97 can be obtained. For the vertical component of rotation rate, the

fit is slightly lower than for strain, but still gives a very good cross-correlation coefficient of 0.95.

### DISCUSSION

The goal of this study was to examine the consistency of rotational and strain observations obtained with direct and array-derived measurement methods. Making use of the unique instrument setting at PFO, we analyzed data of the 2015  $M_w$  6.7 earthquake. The results of the different measurement methods agree very well with overall high correlation coefficients ( $Xcorr \geq 0.95$ ). However, there are small differences between the two observation methods. In the following, we mention sev-



▲ **Figure 4.** Ten out of twelve components of ground motion for the  $M_w$  6.7 Gulf of California earthquake. (a) Translational acceleration of the center station (01) for radial, transverse, and vertical component; (b) three components of rotation rate; (c) four out of six components of strain rate. Rows are drawn to scale according to scaling given in the first column. Array-derived rotation and strain rate are shown in the upper traces (based on entire array). Direct observations for rotation and strain rate are shown in the lower traces. The differences between array-derived observations and direct measurements are plotted in gray, with normalized rms deviation and Xcorr given for each component.

eral causes that might explain the differences theoretically, and discuss whether and how they are applicable to this case study.

First of all, we have to consider the instruments themselves. Both the RLG and the LSM are instruments based on optical principles. They come with advantages such as a high resolution and a uniform transfer function through the massless recording system. The sensitivity of an RLG increases with increasing size. At PFO, the size of the RLG is 1.6 m length (area 2.56 m<sup>2</sup>), quite limited. Nevertheless, it provided us with high-quality data having a high signal-to-noise ratio for the analyzed earthquake (Fig. 4). In addition to the size, also the mechanical rigidity of the entire instrument can influence the measurement quality.

The stable construction and instrument setup makes this effect negligible (e.g., Schreiber *et al.*, 2009).

LSM measurements are limited by the length of the instrument. When the considered wavelength is similar to the length of the instrument, the measured amplitudes get distorted and spatial aliasing occurs (Agnew and Wyatt, 2003). At PFO, the length of the LSM is 732 m, and the minimum wavelength we considered is  $\lambda = 3800/0.32 = 11,875$  m. Therefore, this limitation is not applicable for our experiment.

Second, using translational seismometers for array-derived methods, Suryanto *et al.* (2006) have shown that even very small phase and amplitude uncertainties have a large influence on the

array-derived result. Such uncertainties can be introduced, for example, through uncertainties in the seismometer response function (position of poles and zeros). Effects such as background noise (if not too high), positioning uncertainties of the stations, or uncertainties in the seismometer response (as long as they are the same for all stations) can be neglected. Moreover, [Suryanto et al. \(2006\)](#) showed that the array-derived results can be stabilized significantly when using as many stations as possible, though, in theory, only three stations are needed. In that case, random errors and/or systematic differences cancel out. In this study, we have shown that the largest subarray gives the most stable results for array-derived measurements (Fig. 3). Nevertheless, for the comparison with direct measurements in Figure 4, we used the data of the entire array - that is, 13 stations - to effectively make use of the stabilizing effect of such a high number of stations. In addition, we avoided measurement uncertainties and spatial aliasing by applying an appropriate band-pass filter. The determination of such an appropriate filter probably could be improved when applying higher-order spatial gradient calculation as already mentioned in the section on limitations of the array method.

Third, we have to consider that the RLG measurement is a point measurement, whereas LSM and array-derived measurements provide us with an average over an area of specific extent defined by the instrument geometry and scaling. Thus, effects due to a nonplanar wavefront, local heterogeneities, topography, or other site effects, can bias the resulting measurement. Also, strain-rotation coupling can significantly bias the array-derived measurement of rotation ([van Driel et al., 2012](#)). Taking these facts into account, the cross-correlation coefficient of  $>0.95$  for the direct and array-derived measurements of vertical rotation rate nicely shows the consistency between the two methods. The cross-correlation coefficients for the strain comparison are higher than those for the rotation. One reason could be that both measurements, direct and array derived, are spatial averages and thus influenced by the same biases.

Finally, we want to point out that tilt may affect the array-derived observation if the tilt would be different in different parts of the array. For the considered wavelengths in this study, we assume tilt to be uniform over the area of the complete array. Also, direct measurements using ring lasers are influenced by tilt. However, [Pham et al. \(2009\)](#) have shown that this effect can be neglected as well.

## CONCLUSION

For the first time, translation has been measured collocated with rotation and strain. Using the unique instrument setting of the PFO, we measured 10 out of 12 components of the seismic wavefield. Based on data of the 2015  $M_w$  6.7 Gulf of California earthquake, we compared direct with array-derived measurements. We found that they are greatly consistent, though small differences remain.

The advantages of a direct measurement of rotation and strain, using rotation sensors and strainmeters, are the simple preprocessing of the data due to the unique transfer function and the insensitivity to tilt and translation. In contrast, the

array-derived measurement provides us with a cheap method because seismological arrays already exist worldwide. However, the results are only reliable within a quite limited range of frequencies, depending on the size of the array. Additionally, when no array is available in the region of interest, then, indeed, it is an expensive technique with respect to money and logistics.

Broadband portable rotation sensors are around the corner ([Bernauer et al., 2016](#); [iXblue, 2017](#)) that could complement the bulky but highly sensitive ring laser systems for observatories for local and regional field applications.

## DATA AND RESOURCES

Almost all data are recorded at the Piñon Flat Observatory and are available via International Federation of Digital Seismograph Networks (FDSN) clients (network code PY). Strain data were kindly provided by Frank Wyatt. Data used in Appendix A are from Adam Ringler and are available either via <https://github.com/aringle-usgs/ArrayANAdata> (last accessed February 2017) or via FDSN client Incorporated Research Institutions for Seismology (IRIS), network code GS. Data processing and figure preparation (except Fig. 1) were carried out with the help of ObsPy ([docs.obspy.org](https://docs.obspy.org), last accessed November 2016). Figure 1 was created using the Generic Mapping Tool (GMT) by Paul Wessel and Walter H. F. Smith ([gmt.soest.hawaii.edu/](https://gmt.soest.hawaii.edu/), last accessed November 2016). ☒

## ACKNOWLEDGMENTS

The authors sincerely thank Frank Wyatt for preparing the strainmeter data that made this article possible. The authors greatly appreciate the cooperation of Adam Ringler at Albuquerque Seismological Laboratory. The authors thank him for providing the data used in Appendix A and valuable discussion which helped to improve this article. This study was supported by the European Research Council (ERC-Project: ROMY). C. H. is grateful for support through the Emmy Noether program of the German Research Foundation (DFG, HA7019/1-1). The authors also thank Charles Langston and associate editor for their constructive comments.

## REFERENCES

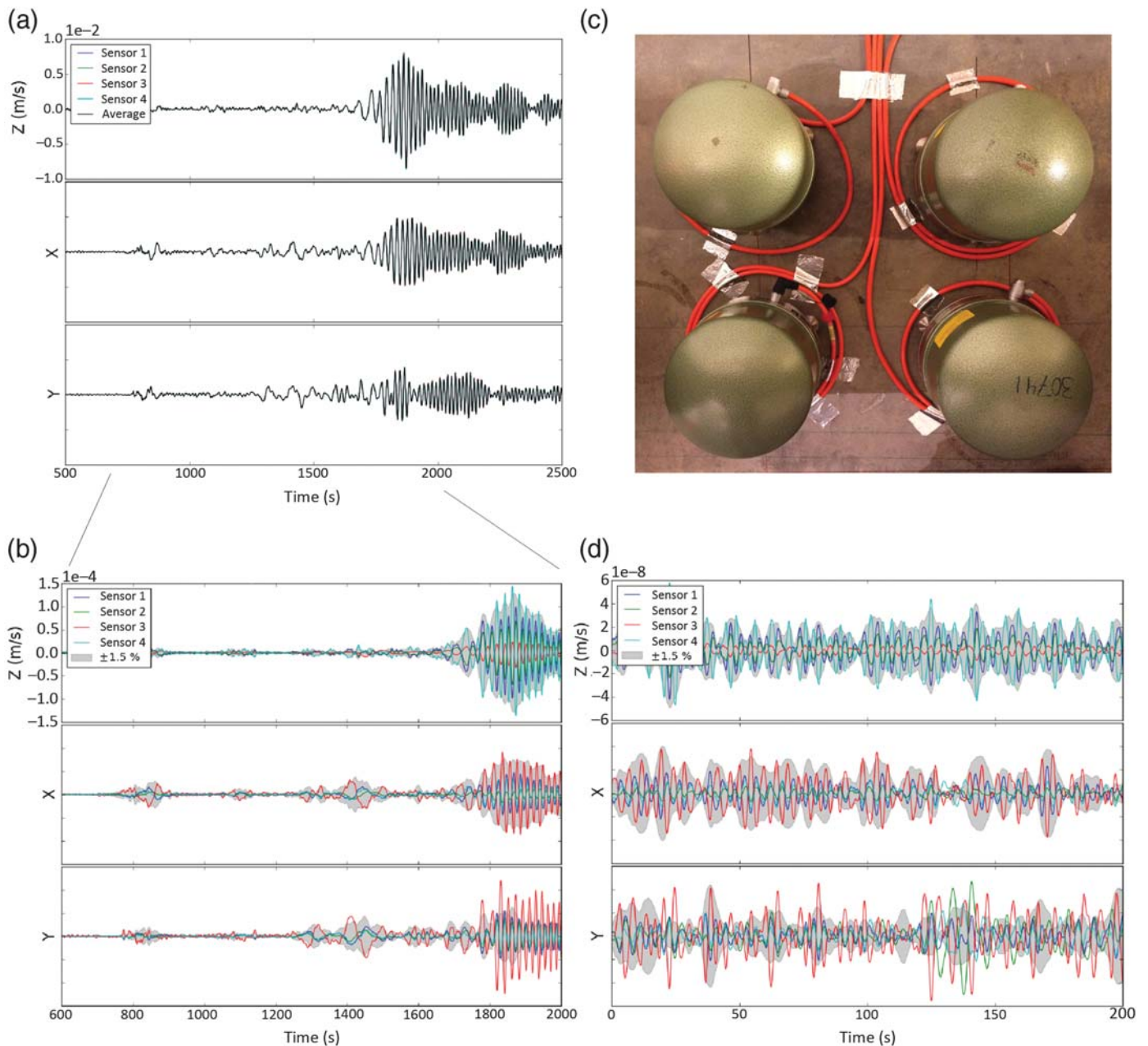
- Agnew, D. C., and F. K. Wyatt (2003). *Long-Base Laser Strainmeter: A Review*, UC San Diego, Scripps Institution of Oceanography, San Diego, California, available at <http://escholarship.org/uc/item/21z72167> (last accessed November 2016).
- Agnew, D. C., and F. K. Wyatt (2014). Dynamic strains at regional and teleseismic distances, *Bull. Seismol. Soc. Am.* **104**, 1846–1859.
- Aki, K., and P. G. Richards (2002). *Quantitative Seismology*, Second Ed., University Science Book, Sausalito, U.S.A..
- Barbour, A. J., and D. C. Agnew (2012). Detection of seismic signals using seismometers and strainmeters, *Bull. Seismol. Soc. Am.* **102**, 2484–2490.
- Berger, J., and R. Lovberg (1970). Earth strain measurements with a laser interferometer, *Science* **170**, 296–303.
- Bernauer, F., J. Wassermann, F. Guattari, and H. Igel (2016). Portable sensor technology for rotational ground motions, *Geophys. Res. Abstr.* **18**, Abstract EGU 2016–13345.

- Bernauer, M., A. Fichtner, and H. Igel (2012). Measurements of translation, rotation and strain: New approaches to seismic processing and inversion, *J. Seismol.* **16**, 669–681.
- Bernauer, M., A. Fichtner, and H. Igel (2014). Reducing nonuniqueness in finite source inversion using rotational ground motions, *J. Geophys. Res.* **119**, 4860–4875.
- Beyreuther, M., R. Barsch, L. Krischer, T. Megies, Y. Behr, and J. Wassermann (2010). ObsPy: A Python toolbox for seismology, *Seismol. Res. Lett.* **81**, 530–533.
- Cochard, A., H. Igel, B. Schuberth, W. Suryanto, A. Velikoseltsev, U. Schreiber, J. Wassermann, F. Scherbaum, and D. Vollmer (2006). Rotational motions in seismology: Theory, observation, simulation, in *Earthquake Source Asymmetry, Structural Media and Rotation Effects*, R. Teisseyre, E. Majewski, and M. Takeo (Editors), Springer, Berlin/Heidelberg, Germany.
- DeWolf, S., F. K. Wyatt, M. A. Zumberge, and D. C. Agnew (2012). Vertical and horizontal optical fiber strainmeters for measuring Earth strain, AGU Fall Meet., Abstracts FM.G23B0918D.
- DeWolf, S., F. K. Wyatt, M. A. Zumberge, and W. Hatfield (2015). Improved vertical and optical fiber borehole strainmeter design for measuring Earth strain, *Rev. Sci. Instrum.* **86**, 114502.
- Donner, S., M. Bernauer, and H. Igel (2016). Inversion for seismic moment tensors combining translational and rotational ground motions, *Geophys. J. Int.* **207**, 562–570, doi: [10.1093/gji/ggw298](https://doi.org/10.1093/gji/ggw298).
- Gomberg, J., and D. Agnew (1996). The accuracy of seismic estimates of dynamic strains: An evaluation using strainmeter and seismometer data from Piñon Flat Observatory, California, *Bull. Seismol. Soc. Am.* **86**, 212–220.
- Hadziioannou, C., P. Gaebler, U. Schreiber, J. Wassermann, and H. Igel (2012). Examining ambient noise using colocated measurements of rotational and translational motion, *J. Seismol.* **16**, 787–796.
- iXblue (2017). blueSeis—a portable, 3-components rotational seismometer, [www.blueseis.com](http://www.blueseis.com) (last accessed May 2017).
- Igel, H., U. Schreiber, A. Flaws, B. Schuberth, A. Velikoseltsev, and A. Cochard (2005). Rotational motions induced by the M 8.1 Tokachi-Oki earthquake, September 25, 2003, *Geophys. Res. Lett.* **32**, L08309, doi: [10.1029/2004GL022336](https://doi.org/10.1029/2004GL022336).
- Krischer, L., T. Megies, R. Barsch, M. Beyreuther, T. Lecocq, C. Caudron, and J. Wassermann (2015). ObsPy: A bridge for seismology into the scientific Python ecosystem, *Comput. Sci. Disc.* **8**, doi: [10.1088/1749-4699/8/1/014003](https://doi.org/10.1088/1749-4699/8/1/014003).
- Langston, C. A. (2007a). Spatial gradient analysis for linear seismic arrays, *Bull. Seismol. Soc. Am.* **97**, 265–280.
- Langston, C. A. (2007b). Wave gradiometry in two dimensions, *Bull. Seismol. Soc. Am.* **97**, 401–416.
- Langston, C. A., and S. Liang (2008). Gradiometry for polarized seismic waves, *J. Geophys. Res.* **113**, no. B08305, doi: [10.1029/2007JB005486](https://doi.org/10.1029/2007JB005486).
- Lin, C.-J., W.-G. Huang, H.-P. Huang, B.-S. Huang, C.-S. Ku, and C.-C. Liu (2012). Investigation of array derived rotation in TAIPEI 101, *J. Seismol.* **16**, 1–11.
- Megies, T., M. Beyreuther, R. Barsch, L. Krischer, and J. Wassermann (2011). ObsPy—What can it do for data centers and observatories, *Ann. Geophys.* **54**, 47–58.
- Pham, N. D., H. Igel, J. Wassermann, A. Cochard, and U. Schreiber (2009). The effects of tilt on interferometric rotation sensors, *Bull. Seismol. Soc. Am.* **99**, 1352–1365.
- Poppiers, C., and E. V. Evans (2015). The effects of measurement uncertainties in seismic wave gradiometry, *Bull. Seismol. Soc. Am.* **105**, 3143–3155.
- Prieto, G. A., J. F. Lawrence, and G. C. Beroza (2009). Anelastic Earth structure from the coherency of the ambient seismic field, *J. Geophys. Res.* **114**, no. B07303, doi: [10.1029/2008JB006067](https://doi.org/10.1029/2008JB006067).
- Reinwald, M., M. Bernauer, H. Igel, and S. Donner (2016). Improved finite-source inversion through joint measurements of rotational and translational ground motions: A theoretical study, *J. Geophys. Res.* **7**, 1467–1477.
- Ringler, A., D. Wildon, T. Storm, B. T. Marshall, C. R. Hutt, and A. Holland (2016). Noise reduction in long-period seismograms by way of array summing, *Bull. Seismol. Soc. Am.* **106**, doi: [10.1785/0120160129](https://doi.org/10.1785/0120160129).
- Romney, C. (1964). Combinations of strain and pendulum seismographs for increasing the detectability of P, *Bull. Seismol. Soc. Am.* **54**, 2165–2174.
- Schreiber, K. U., J. N. Hautmann, A. Velikoseltsev, J. Wassermann, H. Igel, J. Otero, F. Vernon, and J.-P. R. Wells (2009). Ring laser measurements of ground rotations for seismology, *Bull. Seismol. Soc. Am.* **99**, 1190–1198.
- Schreiber, K. U., G. E. Stedman, H. Igel, and A. Flaws (2006). Ring laser gyroscopes as rotation sensor for seismic wave studies, in *Earthquake Source Asymmetry, Structural Media and Rotation Effects*, R. Teisseyre, E. Majewski, and M. Takeo (Editors), Springer, Berlin/Heidelberg, Germany.
- Shearer, P. (2009). *Introduction to Seismology*, Second Ed., Cambridge University Press, Cambridge, United Kingdom.
- Spudich, P., and J. B. Fletcher (2008). Observation and prediction of dynamic ground strains, tilts, and torsions caused by the  $M_w$  6.0 2004 Parkfield, California, earthquake and aftershocks, derived from UPSAR array observations, *Bull. Seismol. Soc. Am.* **98**, 1898–1914.
- Spudich, P., L. K. Steck, M. Hellweg, J. B. Fletcher, and L. M. Baker (1995). Transient stresses at Parkfield, California, produced by the M 7.4 Landers earthquake of June 28, 1992 observations from the UPSAR dense seismograph array, *J. Geophys. Res.* **100**, 675–690.
- Suryanto, W., H. Igel, J. Wassermann, A. Cochard, B. Schuberth, D. Vollmer, F. Scherbaum, U. Schreiber, and A. Velikoseltsev (2006). First comparison of array-derived rotational ground motions with direct ring laser measurements, *Bull. Seismol. Soc. Am.* **96**, 2059–2071.
- Tanimoto, T., C. Hadziioannou, H. Igel, J. Wassermann, U. Schreiber, and A. Gebauer (2015). Estimate of Rayleigh-to-Love wave ratio in the secondary microseism by colocated ring laser and seismograph, *Geophys. Res. Lett.* **42**, 2650–2655.
- van Driel, M., J. Wassermann, M. Fernanda Nader, B. S. A. Schuberth, and H. Igel (2012). Strain rotation coupling and its implications on the measurement of rotational ground motions, *J. Seismol.* **16**, 657–668.
- Velikoseltsev, A. (2005). The development of a sensor model for large ring lasers and their application in seismic studies, *Ph.D. Thesis*, Fakultät für Bauingenieur- und Vermessungswesen, TU Munich, Munich, Germany.
- Wassermann, J., S. Lehndorfer, H. Igel, and U. Schreiber (2009). Performance test of a commercial rotational sensor, *Bull. Seismol. Soc. Am.* **99**, 1449–1456.
- Zumberge, M. A., J. Berger, M. A. Dzieciuch, and R. L. Parker (2004). Resolving quadrature fringes in real time, *Appl. Opt.* **43**, 771–775.

## APPENDIX A

### SEISMOGRAM UNCERTAINTY

Four colocated STS-2 high-gain seismometers at the Albuquerque Seismological Laboratory are used for evaluating the calibration error of seismogram recordings. Two of the seismometers were recorded by the 26-bit resolution channels of Quanterra Q330HR, whereas the other two were recorded by the 24-bit resolution channels of the same digitizer. The recordings are Global Positioning System synchronized.



▲ **Figure A1.** Evaluation of the calibration error from four collocated STS-2 seismometers installed at Albuquerque Seismological Laboratory (ASL). (a) Superposition of all recordings of the  $M_w$  8.8 Chile earthquake band-pass filtered between 0.01 and 1 Hz. (b) Amplitude differences between each recording and the average of all recordings of the Chile earthquake. As a reference, the  $\pm 1.5\%$  range of the envelope of the average amplitude is shown as gray shade. (c) Picture of the experiment setup at ASL. (d) Same as (b) side, just on background noise before the event onset.

We consider two instrument-corrected data sets: data from the 16 September 2015  $M_w$  8.8 Chile earthquake (distance  $77.6^\circ$ ) as well as a background noise before the same earthquake. The superposition of the seismograms is shown in Figure A1a.

We derived an average amplitude from all four recordings and subtracted this average from each recording (Fig. A1b,d). In both cases, for the earthquake and the background noise, the amplitude differences appear to be of similar magnitude on the

vertical as well as on the horizontal components. Therefore, we think the differences are not caused by elevated horizontal noise levels, but due to variations in the sensitivity of the instruments.

By fitting the amplitude envelopes, we found that the largest amplitude difference is more or less within a  $\pm 1.5\%$  range of the average amplitude. Only for the y component of sensor 3, the amplitude difference is clearly exceeding this range in the time window for the Love waves of the event data and partly

<b>Stations</b>	<b>Relative Orientation (°)</b>
BPH01	0
BPH02	-1.4
BPH03	0.3
BPH04	0.1
BPH05	-0.7
BPH06	-0.6
BPH07	-1.9
BPH08	0.4
BPH09	-6.6
BPH10	0.3
BPH11	-1.1
BPH12	-2.6
BPH13	0.2

for the background noise. Therefore, we consider the 1.5% a fair threshold.

A recent study uses the same data to investigate methods for removing long-period noise using collocated sensors (Ringler *et al.*, 2016).

## APPENDIX B

### RELATIVE ORIENTATION

Small differences in seismometer orientation within the array can cause unreliable result for array-derived observations. We estimate the relative orientations of the seismic stations at Piñon Flat Observatory with respect to the central station BPH01 as follows. Let  $\theta$  denotes the relative orientation between the considered sensor and the reference sensor of the central station with counterclockwise motion as the positive rotation. We denote the two orthogonal horizontal components of the sensor as  $x$  and  $y$ . Then, we maximize the following equation for  $\theta$ :

$$X_{\text{corr}}(x', x_{\text{ref}}) + X_{\text{corr}}(y', y_{\text{ref}})$$

with

$$x' = x_{\text{est}} \cos \theta + y_{\text{est}} \sin \theta, \quad y' = -x_{\text{est}} \sin \theta + y_{\text{est}} \cos \theta$$

and  $X_{\text{corr}}$  as the normalized cross-correlation coefficients. The results of the orientation analysis based on data of the  $M_w$  6.7 Gulf of California earthquake are shown in Table B1. All data have been corrected for their misalignment before we applied the array-derivation method.

*Stefanie Donner*  
*Chin-Jen Lin*<sup>1</sup>  
*Céline Hadziioannou*<sup>2</sup>  
*André Gebauer*  
*Heiner Igel*  
*Joachim Wassermann*  
*Department of Earth and Environmental Sciences*  
*Ludwig Maximilian University Munich*  
*Theresienstraße 41*  
*80333 Munich, Germany*  
*donner@geophysik.uni-muenchen.de*  
*lin@geophysik.uni-muenchen.de*  
*hadzii@geophysik.uni-muenchen.de*  
*gebauer@geophysik.uni-muenchen.de*  
*igel@geophysik.uni-muenchen.de*  
*jowa@geophysik.uni-muenchen.de*

*Frank Vernon*  
*Duncan Carr Agnew*  
*Institute of Geophysics and Planetary Physics*  
*Scripps Institution of Oceanography*  
*University of California San Diego*  
*9500 Gilman Drive Number 0225*  
*La Jolla, California 92093-0225 U.S.A.*  
*flvernon@ucsd.edu*  
*dagnew@ucsd.edu*

*Ulrich Schreiber*  
*Forschungseinrichtung Satellitengeodäsie*  
*Technical University of Munich*  
*Fundamentalstation Wettzell*  
*Sackenrieder Straße 25*  
*93444 Bad Koetzing, Germany*  
*ulrich.schreiber@bv.tum.de*

Published Online 24 May 2017

<sup>1</sup> Now at Institute of Earth Sciences, Academia Sinica, Taiwan.

<sup>2</sup> Now at Institute of Geophysics, University of Hamburg, Bundesstraße 55, 20146 Hamburg, Germany; celine.hadziioannou@uni-hamburg.de.